Available online at www.sciencedirect.com
ScienceDirect
Journal of Power Sources 173 (2007) 467–477
JOURNAL OF POWER SOURCES
www.elsevier.com/locate/jpowsour

Analysis of design variables for water-gas-shift reactors by model-based optimization

Javier A. Francesconi, Miguel C. Mussati, Pio A. Aguirre *

INGAR - Instituto de Desarrollo y Diseño, Avellaneda 3657, CP: S3002GJC, Santa Fe, Argentina

Received 15 February 2007; received in revised form 16 April 2007; accepted 17 April 2007
Available online 4 May 2007

Abstract

This work analyzes the water-gas-shift reactor design as component of the CO clean-up system of the ethanol processor for H_2 production applied to PEM fuel cells. The WGS reactor constitutes the element of greater volume of the processor motivating its optimization. A model-based reactor optimization for different reactor configurations permits to obtain both designs for reducing volumes and optimal operating conditions. The heterogeneous model used allows computing the optimal reactor length and diameter, and the optimal catalyst particle diameter. The model computes the constraints required for catalyst, such as maximum and minimum operation temperature. The volume is sensitive to the CO outlet concentration. According to the required CO conversion it is necessary more than one reactor unit for the case study analyzed. When considering the insulating material, there exists an optimal thickness that affects the final volume and the design variables. These results are useful for estimating the minimum and relative sizes that allows conventional reactor technology.

Several reactors configurations are analyzed in order to state the limiting values of the main design variables. Specially, insulation conditions are studied in detail to access minimum total volumes.

Keywords: Optimization; Reactor model; Water-gas shift; Ethanol processor

1. Introduction

During the last decade, there have been important advances in fuel cells technology. Fuel cells are being developed for applications to electrical energy generation and co-generation systems (coupled heat and power) in both stationary and mobile systems. Since fuel cells are high-efficiency energy converter devices and due to their low polluting emission levels, they become more and more attractive as a power generation alternative, specially in transportation industry [1,2].

Direct hydrogen fuel cell systems are clearly the preferred fuel cell operation mode. Nevertheless, the absence of a network for hydrogen distribution, and the risk and difficulties associated with hydrogen storage and transport makes it difficult a widespread use of this alternative. On the other hand, a successful implementation of fuel cells in the short term can be performed by fuel reforming. A promising route consists of the steam reforming of alcohols, mainly methanol and ethanol. The possibility of using ethanol reforming for producing hydrogen as combustible for fuel cells has generated an increased motivation for investigating the reforming process of alcohols [3]. The ethanol shows advantages over fuels derived from fossil sources, since it is a renewable source, and has a neutral effect on the carbon dioxide emissions, and can be obtained by fermentation [4].

In order to generate a hydrogen rich gas stream in the fuel processor, a feeding stream consisting of ethanol and water is converted into a stream with high hydrogen content. Fig. 1 schematizes the global steam reforming process, which is a mature technology for synthesis gas, ammonia and hydrogen production from natural gas.

Proton exchange membrane fuel cell (PEMFC) demands a CO-free hydrogen stream for operation. Since CO is adsorbed on the catalyst surface causing catalyst poisoning, it is necessary to reach CO concentrations less than 10 ppm for preventing irreversible damage and to facilitate the electrochemical reaction on the Pt electrode. The conditioning of the gas stream

* Corresponding author. Tel.: +54 342 453 4451; fax: +54 342 455 3439.
E-mail addresses: javierf@ceride.gov.ar (J.A. Francesconi), mmussati@ceride.gov.ar (M.C. Mussati), paguir@ceride.gov.ar (P.A. Aguirre).

0378-7753/$ – see front matter © 2007 Elsevier B.V. All rights reserved.
doi:10.1016/j.jpowsour.2007.04.048

Nomenclature

a_v	external catalyst surface area per unitary reactor volume (cm^{-1})
A_r	cross reactor area (cm^2)
C_i	component concentration along the reactor ($mol\,cm^{-3}$)
Cp_i	molar heat capacity of i component ($kJ\,mol^{-1}\,°C^{-1}$)
Cp_f	fluid mass heat capacity ($kJ\,g^{-1}\,°C^{-1}$)
$C_{S,i}$	component concentration inside the catalyst pore ($mol\,cm^{-3}$)
$C^S_{S,i}$	component concentration at the external catalyst surface ($mol\,cm^{-3}$)
$D_{eff,i}$	effective diffusivity in porous media ($cm^2\,s^{-1}$)
D_t	reactor tube diameter (cm)
D_p	catalyst particle diameter (cm)
D_{ins}	outer insulation diameter (cm)
e_{ins}	insulating material thickness (cm)
e_t	reactor tube thickness (cm)
F_i	molar flow of component i ($mol\,s^{-1}$)
G	mass flow per unitary reactor area ($g\,cm^{-2}\,s^{-1}$)
h_f	energy transfer coefficient in the film ($kJ\,cm^{-2}\,s^{-1}\,°C^{-1}$)
h_w	energy transfer coefficient ($kJ\,cm^{-2}\,s^{-1}\,°C^{-1}$)
ΔH_j	heat of reaction ($kJ\,mol^{-1}$)
k_g	mass transfer coefficient in the film ($cm\,s^{-1}$)
L_t	reactor length (cm)
M_i	molecular weigth of i component ($g\,mol^{-1}$)
P	pressure (atm)
q_{cv}	convective heat flux ($kJ\,cm^{-2}\,s^{-1}$)
q_{rad}	radiative heat flux ($kJ\,cm^{-2}\,s^{-1}$)
Q^{rx}	heat exchanged between the reactor and its surroundings per unitary bed volume ($kJ\,cm^{-3}\,s^{-1}$)
r_j	reaction rate ($mol\,g\text{-}cat^{-1}\,s^{-1}$)
T_{amb}	environment temperature (°C)
T_f	fluid temperature (°C)
T_{ins}	surface insulating material temperature (°C)
T_S	temperature inside the catalyst pore (°C)
T^S_S	temperature at the catalyst surface (°C)
T_w	reactor wall temperature (°C)
Tc_i	critical temperature for the i component (K)
Tr_i	reduced temperature for the i component
V	volume (cm^3)
Vc_i	critical temperature for the i component ($cm^3\,mol^{-1}$)
X_{CO}	CO conversion

Greek letters

α^i_j	stoichiometric coefficient of component i in reaction j
ε_b	bed porosity
ε_{ins}	insulation surface emissivity
λ_f	gas thermal conductivity ($kJ\,cm^{-1}\,s^{-1}\,°C^{-1}$)
λ_{eff}	effective conductivity inside a particle ($kJ\,cm^{-1}\,s^{-1}\,°C^{-1}$)
μ_f	gas viscosity ($g\,cm^{-1}\,s^{-1}$)
ρ_f	gas phase density ($g\,cm^{-3}$)
ρ_p	catalyst density ($g\text{-}cat\,cm^{-3}$)
σ	Stefan–Boltzmann constant ($5.670 \times 10^{-15}\,kJ\,K^{-4}\,cm^{-2}\,s^{-1}$)

generated from the steam reforming of ethanol is partially performed by the water-gas-shift reaction (WGS). Afterwards, a final CO reduction is performed by the preferential oxidation reactor (CO-PrOx), where the oxidation of carbon monoxide is the desirable reaction. Nevertheless, undesirable combustion of valuable hydrogen also takes place. The reformer, WGS and CO-PrOx reactors are the nucleus of the steam reforming process, and contribute largely to the total volume and weight of the whole system.

For fuel cell applications, a compact, efficient and reliable fuel processor is desirable. Process synthesis and design tasks are similar to other industrial reforming processes. However, the production capacity level required by fuel processors for vehicles or other similar devices is lower compared to industrial processes. Thus, process units of small size and specific designs are required.

Since the WGS reaction rate is slower than the other reactions involved in the steam reforming process, and is limited at high temperatures by the thermodynamic equilibrium [5], the WGS reactor is the largest and heaviest process component.

The aim of this work is focused on investigating the WGS reactor as a process component of a fuel processor for applications in PEM-type fuel cells, and showing how the reactor design using mathematical programming techniques allows computing both reduced volumes and optimal operation conditions. Different reactor configurations, reactor size and relative sizes of the reactor components (insulating material, reactor tube and reactive bed) can be evaluated; moreover, process performance bottlenecks and opportunities for optimization can be identified and analyzed. This knowledge can be used for process improvements such as lower unit weight and costs, and higher global efficiency.

2. Water-gas-shift reaction

The water-gas-shift reaction is widely applied in industry. It is used in the ammonia synthesis and hydrogen production processes from hydrocarbons reforming. Carbon monoxide reacts with water steam according to:

$$CO + H_2O \leftrightarrow CO_2 + H_2 \quad \Delta H^\circ_{298} = -41.1\,kJ\,mol^{-1}$$

In industry, the main objective of the WGS reaction is to increase and to adjust the H_2/CO molar ratio in the synthesis gas, and to remove CO from the off-gas.

The reaction is moderately exothermic and its equilibrium constant decreases with temperature; high conversions are

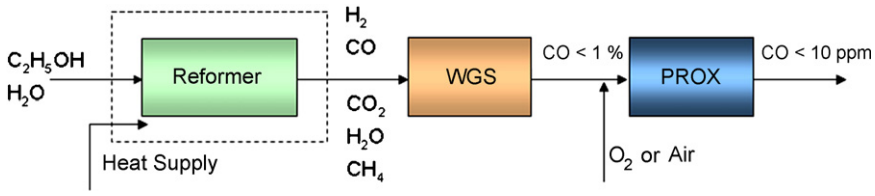

Fig. 1. Scheme of the ethanol processor.

favored at low temperatures. The equilibrium is virtually insensitive to the system pressure. Under adiabatic conditions, conversion in a single catalytic bed is thermodynamically limited. As the reaction progresses the reaction heat increases and the operation temperature limits the conversion. The thermodynamic limitation of the reaction can be overcome using two or more catalytic beds with intermediate cooling, instead of a single bed.

Although the WGS reaction is catalyzed by numerous materials, it is industrially performed in two adiabatic stages using two different catalysts with intermediate cooling. The first stage (high temperature stage HTS) uses an iron-based catalyst (Fe/Cr) operating at 300–450 °C, and it converts the largest amount of CO. Typical CO levels in the outlet stream of a single reactor range between 2% and 4%. The second reactor (low temperature stage LTS) operates at lower temperatures, between 180 °C and 230 °C, using a copper–zinc catalyst supported on alumina Cu/Zn/Al. The LTS stage is favored thermodynamically, and can achieve a residual CO concentration around 0.1–0.3%. The catalyst composition is usually $CuO/ZnO/AlO_3$, being very sensitive to poisoning by chlorides and sulfides, and to sintering. In addition, both catalysts are pyrophorics, i.e., they spontaneously release heat when are exposed to air after activation, increasing the temperature.

In last years, it is noticed a renewed interest for this reaction, motivated by the promising application for coupling the steam reforming of alcohols with fuel cells for power and heat generation systems.

Zalc and Löffler [5] mention that WGS reaction is limited by its intrinsic catalytic activity; therefore, WGS reactor will take up the largest volume in the fuel processor. For a methane processor, the authors estimated a volume of 226 $cm^3\ kW^{-1}$ assuming an optimal temperature profile and for an outlet CO composition of 1% molar.

Using commercial copper-based catalysts, Campbell [6] points out that the reaction is strongly controlled by pore diffusion at 200 °C, and that copper-based catalysts are prone to lose activity due to sintering phenomenon. Thus, the operating temperature range must be limited to 150–250 °C.

The efforts for improving the WGS reactor performance have been focused in a wide spectrum of subjects, including the development of more active catalysts [7–9], experimental and theoretical studies to formulate kinetic expressions for novel catalysts [10–12], and theoretical studies related to heat and mass transfer phenomena in the catalyst particle structure [13]. Research is also concerned with applying and evaluating non-conventional reactors such as microreactors [14], monolith reactors [15] or membrane reactors to carry out the WGS reaction [16].

Giunta at al. [17] apply the one-dimensional heterogeneous model for simulating a WGS reactor using a commercial $Cu/Zn/Ba/Al_2O_3$ catalyst. Based on simulation outputs, the authors recommend adiabatic operation of the reactor.

In this paper a heterogeneous catalytic reactor model used for simulation and optimization is presented. Three different reactor structures are modeled as optimization problems and solved as study cases; specifically, it is addressed the optimal design and operation of: (a) a single adiabatic reactor, (b) two adiabatic reactors with intermediate cooling, and (c) reactor plus its insulation system. In addition, the effect of catalyst deactivation, changes on production scale and pressure effect over the design are analyzed.

2.1. Mathematical model

In this work, the reactor design is performed based on the one-dimensional heterogeneous model. This model offers higher accuracy for reactor design [18]. The mass, momentum and energy balances for the fluid phase and balances for catalyst particles are represented by Eqs. (1)–(7):

Reactor model

Fluid phase

Mass balance

$$-\frac{\mathrm{d}F_i}{\mathrm{d}z} = A_\mathrm{r} k_\mathrm{g} a_\mathrm{v} (C_i - C^\mathrm{S}_{\mathrm{S},i}) \tag{1}$$

B.C. : $z = 0 \quad F_i = F_i^0$

Energy balance

$$G\mathrm{Cp}_\mathrm{f} \frac{\mathrm{d}T_\mathrm{f}}{\mathrm{d}z} = h_\mathrm{f} a_\mathrm{v} (T^\mathrm{S}_\mathrm{S} - T_\mathrm{f}) - Q^\mathrm{rx} \tag{2}$$

B.C. : $z = 0 \quad T_\mathrm{f} = T_\mathrm{f}^0$

Momentum balance (pressure drop along the catalytic bed)

$$-\frac{\mathrm{d}P}{\mathrm{d}z} = \frac{G^2}{\rho_\mathrm{f} D_\mathrm{p}} \frac{(1-\varepsilon_\mathrm{b})}{\varepsilon_\mathrm{b}^3} \left[1.75 + 4.2\, Re^{5/6} \frac{(1-\varepsilon_\mathrm{b})}{Re} \right] \tag{3}$$

B.C. : $z = 0; \quad P = P^0$

(Spherical) catalyst particle

Mass balance

$$\frac{1}{\xi^2} \frac{\mathrm{d}}{\mathrm{d}\xi} \left(D_{\mathrm{eff},i} \xi^2 \frac{\mathrm{d}C_{\mathrm{S},i}}{\mathrm{d}\xi} \right) - \rho_\mathrm{p} \sum_{j=1}^{\mathrm{Nrx}} \alpha_j^i r_j (C_\mathrm{S}, T_\mathrm{S}) = 0 \tag{4}$$

B.C. : $\xi = 0; \quad \dfrac{\mathrm{d}C_{\mathrm{S},i}}{\mathrm{d}\xi} = 0$

$$\xi = \frac{D_p}{2}\begin{cases} C_{S,i} = C^S_{S,i} \\ k_g(C^S_{S,i} - C_i) = -D_{eff,i}\left.\dfrac{dC_{S,i}}{d\xi}\right|_{D_p/2} \end{cases} \quad (5)$$

Energy balance

$$\frac{1}{\xi^2}\frac{d}{d\xi}\left(\lambda_{eff}\xi^2\frac{dT_S}{d\xi}\right) + \rho_p\sum_{j=1}^{Nrx}(-\Delta H)_j r_j(C_S, T_S) = 0 \quad (6)$$

$$\text{B.C.} : \xi = 0; \quad \frac{dT_S}{d\xi} = 0$$

$$\xi = \frac{D_p}{2}\begin{cases} T_S = T^S_S \\ h_f(T^S_S - T_f) = -\lambda_{eff}\left.\dfrac{dT_S}{d\xi}\right|_{D_p/2} \end{cases} \quad (7)$$

Eqs. (5) and (7) represent the mass and energy balances for the fluid-particle interphase, formulated as boundary conditions. In Eq. (2), Q^{rx} is the heat exchanged between the reaction system and its surroundings. In the adiabatic operation mode $Q^{rx} = 0$. When insulation is incorporated into the model, this term evaluates the heat transferred to the environment.

Correlations for the fluid heat capacity (Cp_f), viscosity (μ_f) and thermal conductivity (λ_f) are those given in [19,20] (see Appendix A). Correlations for the mass and energy transfer coefficients in the film (k_g and h_f, respectively), as well as expressions to estimate the effective diffusivity in porous media ($D_{eff,i}$) are those given in [21]. Gas ideal behavior is assumed to evaluate the mixture density of the gas phase (ρ_f). The average molecular weight of the gaseous mixture and the molar flow entering the reactor were used to compute the mass flow per unitary area (G). Heat transfer coefficients are those given in [22].

The bed porosity (ε_b) is estimated by the expression given in [22]:

$$\varepsilon_b = 0.38 + 0.073\left[1 - \frac{(D_t/D_p - 2)^2}{(D_t/D_p)^2}\right] \quad (8)$$

For spherical shape particles, the external catalyst surface area per unitary reactor volume (a_v) is computed by $a_v = 6(1-\varepsilon_b)/D_p$.

Summarizing, molar flow of component i (F_i), fluid temperature (T_f) and pressure along the reactor bed (P) are calculated from differential Eqs. (1)–(3). Component concentration ($C^S_{S,i}$) and temperature (T^S_S) at the external catalyst surface and inside the catalyst pore ($C_{S,i}$, T_S) are obtained from Eqs. (4)–(7).

A fully developed flow is considered at the reactor intake. However, it should be taken into account that the flow into the fixed-bed reactor is generally achieved by means of a feed pipe and a distribution hood. These must therefore be constructed so that the fixed bed is uniformly traversed, and the gas residence time in each flow path of the fixed bed is the same. The effects of the entrance length and the reactor hood design to achieve the uniform gas flow to the catalyst bed are not considered by the model.

2.2. Optimization model

The optimization problem is formulated to obtain the optimal operating conditions and equipment size aiming at minimizing the system volume. Following, the optimization problem is formulated, i.e. the objective function, decision variables and constraints are specified.

Objective function	Min (V_{total})
Decision variables	T^0, L_t, D_t, D_p, e_{ins}
Interior point constraints	
Catalyst temperature	$150\,^\circ\text{C} \le T_s \le 250\,^\circ\text{C}$
External insulator temperature	$T_{ins} \le 60\,^\circ\text{C}$
Final point constraints	
Admissible pressure drop	$(P^0 - P^S)/P^0 \le 0.3$
CO molar fraction	$y_{CO} \le 0.003$
Design constraints	
Plug flow condition	$L_t/D_p > 30$; $D_t/D_p > 10$

As mentioned, it is intended to minimize the total volume of the system. In WGS reactor, the total volume is determined by the volume occupied by the catalyst bed and the volume occupied by the insulating material. The optimization problem determines the optimal reactor length (L_t), reactor diameter (D_t), catalyst particle diameter (D_p), and insulating material thickness (e_{ins}) that minimize the total system volume. For adiabatic operation case, the constraints corresponding to the insulating material temperature (T_{ins}) and insulation thickness (e_{ins}) as decision variable are not included into the model.

Due to the exothermic nature of the WGS reaction it is desirable to keep the reactor temperature within a certain operating range. An upper temperature bound is set for avoiding catalyst sintering. At low temperature, the reaction rate diminishes, the kinetic expression is not longer valid, and water condensation occurs. Then, it is necessary to impose a lower temperature bound. The reactor inlet temperature (T_0) is a decision variable, and its value results from the optimization problem.

The resulting partial differential algebraic equations (PDAEs) are implemented and solved using gPROMS (general Process Modeling System) [23]. gPROMS is a general purpose modeling, simulation and optimization system software. PDAEs are systems of equations that, when are discretized in spatial directions (using any of the traditional numerical methods), result in differential algebraic equations (DAEs). DAEs are essentially sets of ordinary differential equations (ODEs) where some of the variables are constrained by algebraic relations. Then, the resulting initial value DAE problem is integrated in the z direction present in the system.

The algorithm used in gPROMS for solving the differential equation system is based on a backward differentiation formula (BDF) type method. The composition and temperature profiles established inside the catalyst particle, are obtained by discretizing Eqs. (6) and (7) using orthogonal collocation on finite element method. Finally, the optimization algorithm used is the single-shooting method, which is also available in gPROMS environment.

2.3. Kinetic model

The reactor is optimized considering the most probable conditions for the WGS reaction in a small-scale ethanol reformer using a commercial $Cu/ZnO/AlO_3$ catalyst from Sud-Chemie. The kinetic expression used is that provided by Choi and Stenger [11]:

$$r_{CO} = 82.2 \exp\left(-\frac{47400}{RT}\right)\left(P_{CO}P_{H_2O} - \frac{P_{CO_2}P_{H_2}}{k_{eq}}\right) \quad (9)$$

where $k_{eq} = P_{CO_2}P_{H_2}/P_{H_2O}P_{CO}$, and can be computed from expressions given in [11].

3. Results and discussion

If a fuel processor for generating 1 kW of power is assumed, 33.3 mol h^{-1} of hydrogen is required [11]. This production rate can be reached if about 10 mol h^{-1} of ethanol is processed in the steam reformer operating at 700 °C with a water/ethanol molar ratio of 4.0. The molar flow rate values of the reformed gases obtained at these operating conditions are the ones reported in [24]. These values are assumed to be the input specifications to the WGS unit. A heat exchanger is needed for reducing the gas temperature to the operating range for favoring the WGS reaction. Thus, the WGS reactor's inlet temperature is a decision variable that results from the optimization problem. The molar flow rates and compositions entering to the WGS reactor are listed in Table 1.

3.1. Adiabatic reactor

Firstly, the adiabatic operation of a single-stage reactor is considered. Three design goals for the outlet CO concentration are specified: 1, 0.7 and 0.3% for each case. Although the CO-PrOx reactor can operate with gaseous mixtures with CO concentration ranging between 0.2% and 2.0%, a design goal of 0.3% may assure good system efficiency.

Since hydrogen is generated by the WGS reaction but is undesirably consumed during the oxidation of CO in the CO-PrOx reactor, there exists a trade-off between the ethanol processor efficiency and the volumes of both reactors. Consequently, an integrated analysis considering both aspects is necessary to find out the suitable CO conversion target in the WGS unit.

The heterogeneous model allows computing the main variables of the system geometry (e.g. optimal reactor length and diameter, and optimal catalyst particle diameter) as well as the main operation variables—e.g. optimal inlet reactor temperature restricted to the thermal profile imposed for avoiding material deterioration. The optimization results obtained are included in Table 2.

Table 1
Inlet molar flow rates and compositions to the WGS reactor

Molar flow rate (mol h^{-1})		Molar fraction	
F_{CH_4}	4.7	y_{CH_4}	0.057
F_{H_2}	36.0	y_{H_2}	0.435
F_{CO}	6.6	y_{CO}	0.080
F_{H_2O}	26.4	y_{H_2O}	0.319
F_{CO_2}	9.1	y_{CO_2}	0.110

Table 2
Optimization results for a single-stage adiabatic WGS reactor

CO output (%)	0.30	0.70	1.00
L_t (cm)	36.50	10.00	10.90
D_t (cm)	7.20	7.39	6.39
D_p (cm)	0.05[a]	0.05[a]	0.05[a]
T^0 (°C)	127.1	164.8	168.7
Volume (cm^3)	1460	432	339

[a] The calculated value corresponds to the lower bound.

It is known that there exists a relationship between the catalyst particle diameter and the pressure drop along the catalytic bed. As the catalyst particle diameter decreases, the mass transfer resistance inside the porous matrix of the catalyst decreases, whereas the system pressure drop increases along the catalytic bed. For almost all analyzed cases, the calculated particle diameter D_p is 0.05 cm, which is the lower bound value assigned to this decision variable in the optimization problem. From the point of view of kinetics and diffusions aspects, the use of small particles favors the reactor performance. Then, the diameter of the cross section of the reactor should be large enough to fulfill the pressure drop constraint imposed. For all analyzed cases, the pressure drop is about 0.1% with respect to the inlet pressure (1 atm). This value is negligible compared to the maximum pressure drop usually accepted and specified in the optimization model (30%).

An increase of the reactor temperature is thermodynamically unfavorable for the water-gas-shift reaction. In adiabatic operation mode, for achieving a CO composition of 0.7% in the outlet reactor stream, an increase of the reactor volume about 30% is needed with respect to reach 1.0% of CO in the off-gases; whereas a reaction volume increment around 330% is needed to reach a CO composition of 0.3%. If a higher CO conversion is required, a lower inlet temperature is needed in order to keep the temperature profile along the reactor below the maximum permitted value.

In order to achieve the goal of 0.3% of CO composition using a single-stage unit operating in adiabatic mode, it was necessary to diminish the lower bound imposed to the operation temperature to 127 °C. It means that a reactor design that fulfills all process, design and operation constraints imposed, is not feasible as the problem was originally formulated.

Fig. 2 shows the simulation results corresponding to the optimal reactor design for a CO composition of 0.3% in the off-gas stream. The temperature and CO molar fraction profiles along the reactor axis are depicted. It can be observed that the reactor volumes to achieve 1.0% and 0.7% of CO concentration in the off-gas are larger compared to the volumes computed by optimization when those concentrations are specified as design constraints.

3.2. Two adiabatic reactors in-series

An alternative arrangement to achieve a final CO composition of 0.3% in the off-gas stream, keeping the reactor temperature

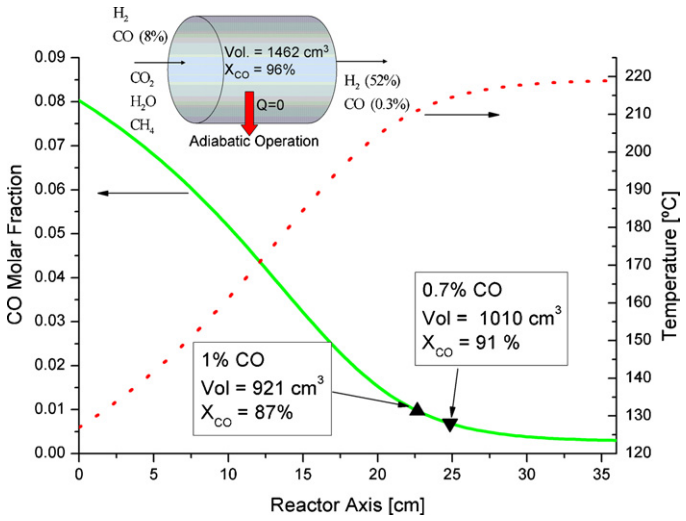

Fig. 2. Simulation results for the design of a final CO concentration of 0.3%.

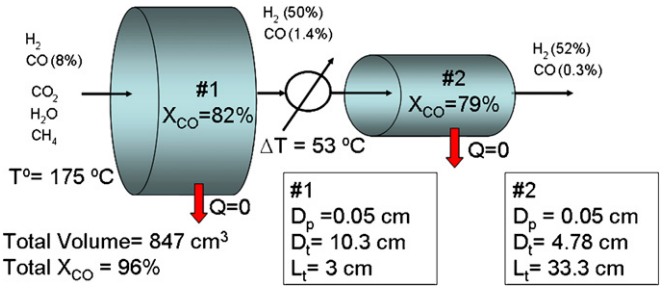

Fig. 3. Optimization results with two adiabatic catalytic beds in-series.

in the desired operation range, is to consider two catalytic beds in series with an intermediate cooling unit (Fig. 3).

To formulate this problem, a new decision variable has to be considered: the inlet temperature to the second catalytic bed. Fig. 3 shows the results obtained from the optimization problem, while Fig. 4 shows the simulated temperature and composition profiles along the whole system.

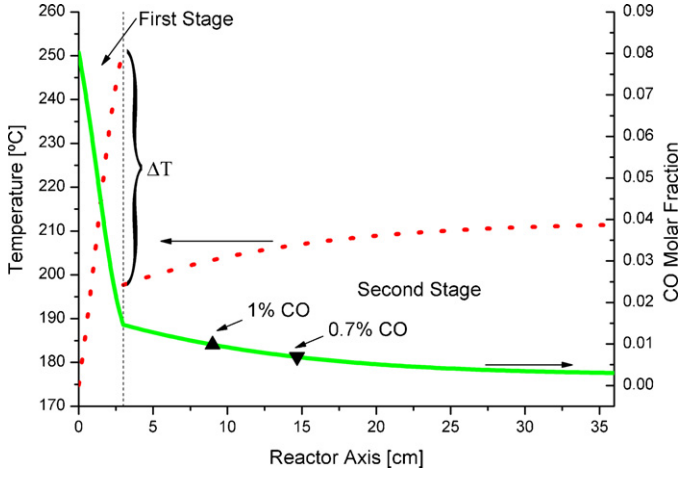

Fig. 4. Temperature and CO molar fraction profiles along the catalytic beds.

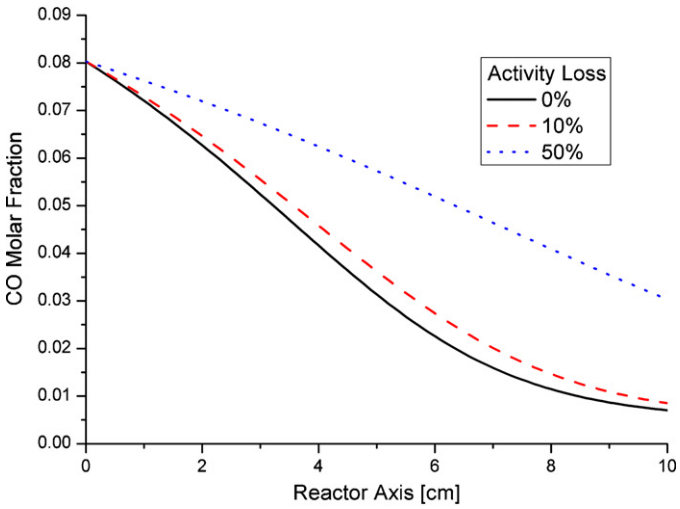

Fig. 5. CO molar fraction profile for different catalyst deactivation levels.

The total volume computing both catalytic beds (847 cm^3) is smaller compared to the volume resulting from a single unit (1462 cm^3). However, it should be noted that the volume occupied by the heat exchanger is not evaluated. The heat exchanger design will depend on the cooling fluid used which may be available from the process streams involved in the global process favoring the system energy integration, and resulting in an increased process efficiency.

In addition, this reactor configuration model allowed finding a reactor design that reaches the desired CO level (0.3%) without diminishing the temperature below 150 °C, value fixed as the lower operating limit.

3.3. Catalyst deactivation

Catalyst deactivation was not considered in the previous reactor configuration designs. The catalyst used showed an activity loss of 10% for a 250 h operation period [11]. Fig. 5 plots simulation results for different catalyst deactivation levels considering the design obtained for the adiabatic reactor to achieve a CO molar fraction of 0.7%. It can be observed that when the activity loss increases the reactor is not being able to fulfill the desired conversion. However, in practice, the effect of the activity loss can be compensated by increasing the inlet reactor temperature. Table 3 shows optimization results when catalyst deactivation is taken into account at the reactor design stage.

Table 3
Optimal reactor design considering catalyst deactivation

Activity loss (%)	0	10	50
CO output (%)	0.70	0.70	0.70
L_t (cm)	10.00	10.00	14.84
D_t (cm)	7.39	7.79	8.46
D_p (cm)	0.05[a]	0.05[a]	0.05[a]
T^0 (°C)	164.8	164.9	164.7
Volume (cm^3)	432	476	833

[a] Computed value is at the lower bound value.

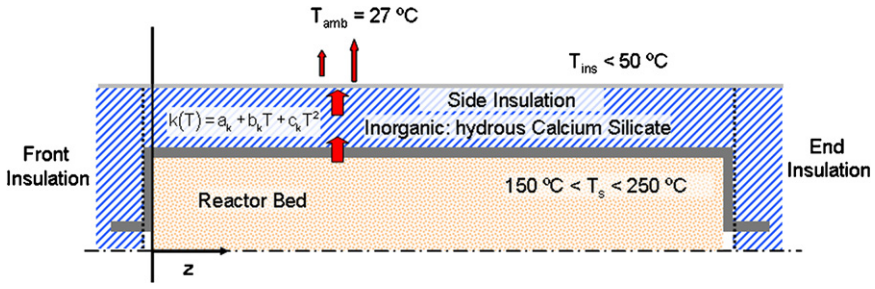

Fig. 6. Scheme of the reactor+insulator system.

3.4. Thermally insulated reactor

In practice, adiabatic operation is performed by attaching an insulating material layer to the wall of the reactor tube for preventing heat loss to surroundings. To analyze its influence on the final size and reactor behavior, heat loss rate to the environment is included into the heterogeneous reactor model.

For a tubular reactor where a reversible exothermic reaction takes place, it is known that the maximum conversion is obtained by a unique temperature profile that maximizes the reaction rate at every point along the reactor. Specifying an adequate extent of insulation represents a pragmatic approach to affect the optimal heat exchange, and thereby to approximate the optimum temperature profile [25].

The insulating material used in the model consists of a layer of calcium silicate covered with a thin layer of aluminum. The heat loss rate to surroundings is modeled as an energy transfer phenomenon by heat conduction through materials involved, and by convection and radiation from material surface to environment (see Appendix B). The insulating material conductivity is considered as a quadratic function of temperature according to the correlation $k(T) = a_k + b_k\ T + c_k\ T^2$. Heat loss by convection and radiation are evaluated by expressions given by Koenig [26]. Three insulations can be localized; side insulation, which depends on reactor wall temperature; front and end insulations, which depend on input and output reactor temperatures, respectively (see Fig. 6). Front and end-insulation were calculated considering the whole surface determined by the reactor-insulation outer diameter. Consequently, possible effects due to the feed pipe to the reactor were not considered.

Owing to that the thickness of commercial-steels tube increases with the diameter, it is necessary to model this behavior to penalize this effect on the total volume. A quadratic expression of the thickness tube as function of the internal diameter is considered ($e_t = a + bD_t + cD_t^2$). This correlation was obtained by fitting data from commercial tubes.

The optimization variable set considered involves the same variables as in the adiabatic case plus the thickness of the insulating material to minimize the total volume of the system (reactor plus insulator), keeping a suitable outer wall temperature.

Firstly, a case with only side insulation is considered. Table 4 summarizes the optimization results for different outer wall temperature values. The insulator thickness is a key decision variable that affects the equipment size. If the outer wall temperature T_{ins} is restricted to values lower than 60 °C, the total volume of the system is 1760 cm^3. Although the total volume (catalytic bed plus insulator) is larger than that computed for a single adiabatic reactor, the volume of the reactive catalytic bed itself is smaller.

Fig. 7 shows temperature and CO molar fraction profiles for two design cases ($T_{ins} < 50$ °C and $T_{ins} < 120$ °C). The total heat loss in each case is about 15 W and 60 W, respectively. If a higher insulator wall surface temperature is allowed, the total volume is reduced to 955 cm^3. It can be observed from Table 4 that for the cases where the outer temperature is limited to values higher than 80 °C there is no need for an insulating material, i.e. the calculated insulator thickness value is at its lower bound (0.001 cm) and the outer reactor metallic tube wall reaches that temperature.

These results indicate, as it is known, that losing heat to surroundings favors the equipment design, i.e. a reduced size is

Table 4
Optimization results for the reactor–insulator system (side insulation only)

T_{ins} (°C)	<50.00	<60.00	<80.00	<120.00
CO Output (%)	0.30	0.30	0.30	0.30
L_t (cm)	18.60	13.31	15.56	25.36
D_t (cm)	9.66	11.00	9.00	6.00
D_p (cm)	0.05[a]	0.05[a]	0.05[a]	0.05[a]
e_{ins} (cm)	1.72	0.37	0.001[a]	0.001[a]
T^0 (°C)	148.5	148.7	154.9	187.5
Bed vol. (cm^3)	1360 (46%)	1260 (72%)	990 (79%)	720 (75%)
Tube vol. (cm^3)	350 (12%)	310 (17%)	270 (21%)	240 (25%)
Ins. vol. (cm^3)	1260 (42%)	190 (11%)	0 (0%)	0 (0%)
Total vol. (cm^3)	2970	1760	1260	960

[a] Computed value is at the lower bound value.

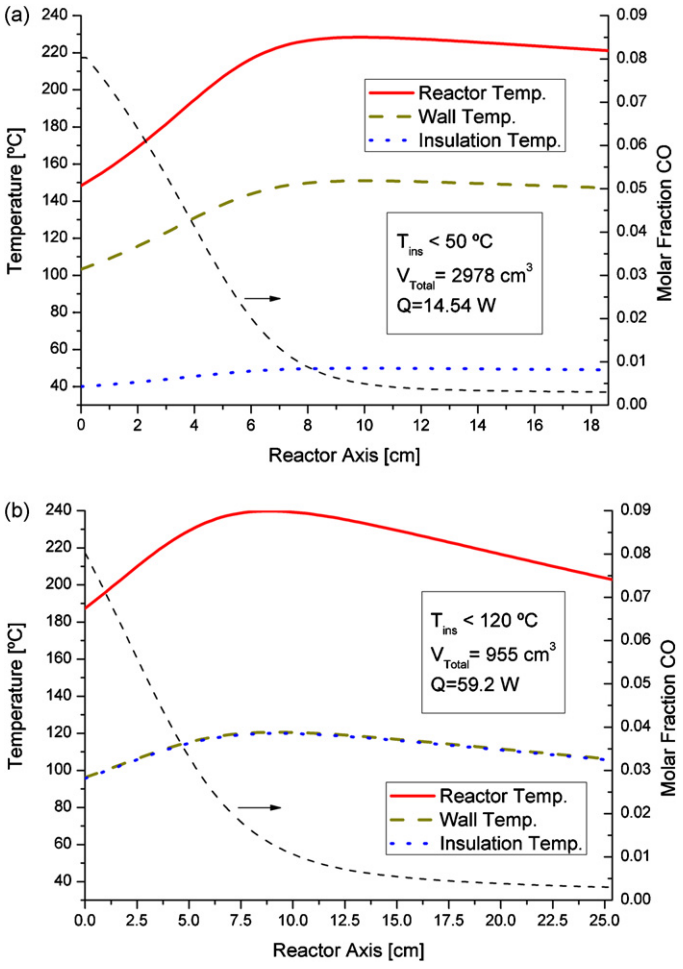

Fig. 7. Temperature and CO molar fraction reactor profiles: (a) $T_{ins} < 50\,^{\circ}C$ and (b) $T_{ins} < 120\,^{\circ}C$.

computed because the reaction is favored by thermodynamic effects. Moreover, a small heat loss diminishes the reactive bed volume compared to an adiabatic reactor.

The effect of considering front and end insulation over the system design is shown in Table 5. The thickness of these insulation sections depend on the inlet and outlet reactor temperature. When the problem considers these sections the optimization results vary slightly, showing smaller reactor diameters.

In order to verify the validity of the 1-D heterogeneous model used at the design stage (optimization model), simulation results are compared to simulation outputs obtained using a 2-D pseudo homogenous model. Fig. 8 depicts the temperature and CO molar composition profiles for the reactor design obtained adopting a maximum outer wall temperature of 50 °C. The difference between the radial average values from the 2-D model and those predicted by the 1-D model is negligible. This agrees with the analysis performed by Kovenklioglu and DeLancey applied to a SO_2 converter [25]. By means of a parametric analysis of the Nusselt number and using simplified models they showed that both 1-D and 2-D models predict approximately the same optimum thickness value.

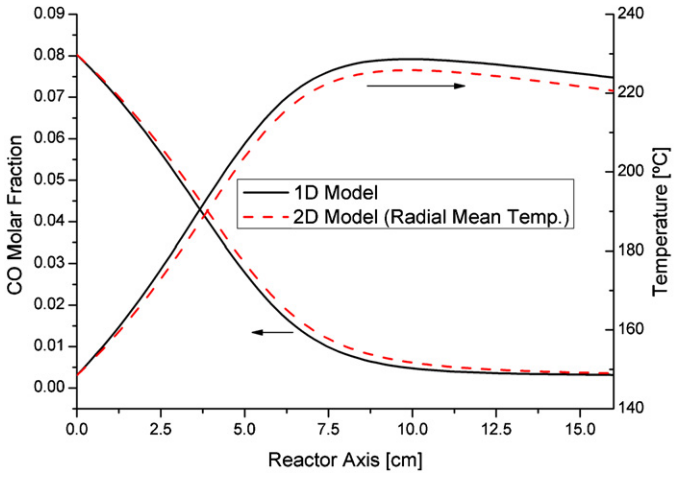

Fig. 8. Comparison between 1-D heterogeneous model and 2-D pseudo homogenous model (radial average values).

3.5. Effect of the change on the production scale

Table 6 lists the optimization results for larger production scale of the processor to reach different power generation targets.

It is worth to note that the model predicts an increase in the particle diameter when increasing the hydrogen production (25 kW and 50 kW cases). As the flow rate of the reactive mixture increases, a particle size increment is computed to maintain an admissible pressure drop through the reactor.

These results indicate that a single reactor processing a flow rate for a power generation target of 50 kW would need for a volume 70% larger than five reactors in parallel of 10 kW each. This behavior is owed to the diffusional resistance when increasing the particle size, decreasing the catalyst effectiveness as can be seen in Fig. 9. The effectiveness factor along the reactor axis for different designs is depicted in Fig. 9. Table 6 shows the activity loss due to diffusional resistance, the catalyst volume (bed volume) per unit of kW generated increases with the target power.

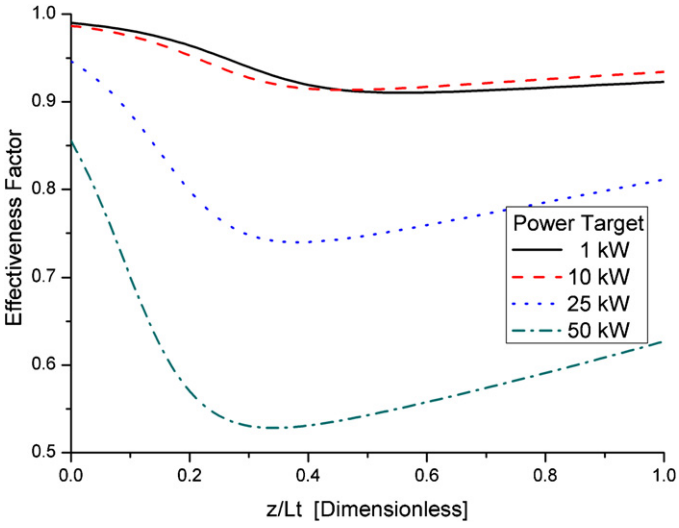

Fig. 9. Effectiveness factor vs. dimensionless reactor length.

Table 5
Optimization results for the reactor–insulator system (side, front and end insulations)

T_{ins} (°C)	<50.00	<60.00	<80.00	<120.00
CO output (%)	0.30	0.30	0.30	0.30
L_t (cm)	22.23	15.02	15.71	25.54
D_t (cm)	8.14	9.82	8.95	5.99
D_p (cm)	0.05[a]	0.05[a]	0.05[a]	0.05[a]
e_{ins} (cm) Side	2.02	0.63	0.001[a]	0.001[a]
e_{ins} (cm) Front	2.22	1.31	0.64	0.32
e_{ins} (cm) End	4.68	2.88	1.34	0.40
T^0 (°C)	148.7	148.5	154.3	187.2
Bed vol. (cm^3)	1160 (29%)	1140 (50%)	990 (70%)	720 (73%)
Tube vol. (cm^3)	330 (08%)	290 (13%)	270 (19%)	240 (24%)
Ins. vol. (cm^3)	2530 (63%)	840 (37%)	160 (11%)	30 (03%)
Total vol. (cm^3)	4020	2270	1420	990

[a] Computed value is at the lower bound value.

Table 6
Optimal reactor designs for different power generation targets (side insulation only)

Power target (kW)	1	10	25	50
T_{ins} (°C)	<50.00	<50.00	<50.00	<50.00
CO output (%molar)	0.30	0.30	0.30	0.30
L_t (cm)	18.60	105.58	207.23	317.75
D_t (cm)	9.66	13.40	17.75	24.28
D_p (cm)	0.05[a]	0.05[a]	0.11	0.16
e_{ins} (cm)	1.72	1.65	2.10	2.32
T^0 (°C)	148.5	149.1	149.2	149.2
Bed vol. (cm^3)	1260 (72%)	14880 (55%)	51260 (57%)	147180 (63%)
Tube vol. (cm^3)	310 (17%)	3240 (12%)	9270 (10%)	19990 (09%)
Ins. vol (cm^3)	190 (11%)	8990 (33%)	29190 (33%)	65410 (28%)
Total vol. (cm^3)	1770	27100	89710	232570
Bed vol. per kW	1260	1490	2050	2940
Total vol. per kW	1770	2710	3590	4650

[a] Computed value is at the lower bound value.

In conclusion, it is convenient to combine reactors in parallel using smaller particle diameters.

For two reactors with intercooler the results do not show a particle increment (Table 7). The temperature decrease between reactors allows achieving a design that satisfies the admissible pressure drop and temperature constraints without increasing the particle diameter.

3.6. Pressure effect on reactor design

Previous results were obtained considering 1 atm as pressure design because of kinetic expression was determined for that condition [12]. As commented by Giunta et al. [16] the CO conversion is favored when pressure increases. The kinetic expression used in this work depends quadratically with pressure. An operating pressure increment favors the

Table 7
Two-stage reactor design with insulations for 1 kW and 50 kW

Power target (kW)	1		50	
T_{ins} (°C)	<50.00		<50.00	
CO output (%)	0.30		0.30	
Reactor stage	#1	#2	#1	#2
L_t (cm)	5.97	6.24	20.07	25.13
D_t (cm)	13.88	6.36	39.00	29.31
D_p (cm)	0.05[a]	0.05[a]	0.05[a]	0.05[a]
e_{ins} (cm) Side	0.58	1.24	2.26	2.14
e_{ins} (cm) Front	2.27	2.58	3.25	4.37
e_{ins} (cm) End	5.35	2.46	7.18	4.47
T^0 (°C)	148.00	164.80	164.63	195.74
Bed vol. (cm^3)	900 (31%)	200 (23%)	23970 (47%)	16950 (50%)
Tube vol. (cm^3)	190 (07%)	60 (07%)	3150 (06%)	2390 (07%)
Ins. vol. (cm^3)	1790 (62%)	590 (69%)	68110 (46%)	14420 (43%)
Total vol. (cm^3)	2880 (77%)	850 (23%)	47330 (60%)	33760 (40%)
Total vol. #1+ #2	3730 cm^3		84510 cm^3	

[a] Computed value is at the lower bound value.

reaction rate and the required bed volume is appreciably diminished. The total reactor volume at 1 atm is 4060 cm^3 (Table 5). By varying the pressure design to 4 atm the total volume computed is 1960 cm^3 for the same design conditions. The volume is significantly diminished (around 52%).

However, the kinetic parameters were obtained at atmospheric conditions; so, this behavior could not be exact. The pressure dependence of the kinetic rate expression used in the model needs further verification. In order to obtain more realistic results it is necessary to determine kinetic data at different operation pressure values.

4. Conclusions

The results of this work show how model-based optimization at the design stage allows estimating efficiently the unit size of the WGS reactor, which is a critical component of ethanol processors, and optimizing the operating conditions. The methodology here applied is robust and can be used in a wide range of design cases.

The WGS reactor is the largest and heaviest component because the WGS reaction is relatively slow compared to the other reactions involved in the whole reforming process, and is inhibited at high temperatures due to the thermodynamic equilibrium.

The heterogeneous model allows computing the optimal reactor length and diameter, the optimal catalyst particle diameter, as well as the inlet reactor temperature of gaseous mixture for adiabatic operation mode.

At the conditions here investigated, the results show that, it is necessary more than one adiabatic catalytic bed in order to achieve the specified conversion with the catalyst temperature imposed. However, if at the design stage, sizing is performed computing the reactive catalytic bed together with the insulating material it is possible to reach the design goal in a single unit. A suitable insulation material thickness may reduce the reactor volume since that heat loss to surroundings favors the reaction conversion.

Although the results of the proposed optimization model depend on the catalyst characteristics and input and output conditions, the methodology and preliminary results obtained from this work are expected to be useful for process design, optimization and control of commercial fuel processors for producing and purifying hydrogen for PEM fuel cells.

Acknowledgments

The financial support from the Consejo Nacional de Investigaciones Científicas y Técnicas (CONICET), Agencia Nacional para la Promoción de la Ciencia y la Tecnología (ANPCyT) and the Universidad Nacional del Litoral of Argentina is acknowledged.

Appendix A. Estimation methods for gas mixture properties

A.1. Viscosity

The Bromley and Wilke modification of the theoretical Hirschfleder method was used to estimate the pure component viscosity (see Perry and Chilton [20]):

$$\mu_i = \frac{33.3\sqrt{M_i \mathrm{Tc}_i}}{\mathrm{Vc}_i^{2/3}} \left(1.058\mathrm{Tr}_i^{0.645} - \frac{0.261}{(1.9\mathrm{Tr}_i)^{0.9\log_{10}(1.9\mathrm{Tr}_i)}} \right)$$

The gas mixture viscosity was calculated from Wilke's method (Reid et al. [19]):

$$\mu_\mathrm{f} = \sum_i \left[y_i \mu_i \left(\sum_j y_j \phi_{ij} \right)^{-1} \right]$$

where $\varphi_{ij} \cong \varphi_{ji}{}^{-1} = (M_j M_i{}^{-1})^{1/2}$, as given by Herning and Zipperer (Reid et al. [19]).

A.2. Thermal conductivity

The pure component thermal conductivities were calculated using the Eucken's approximantion (Perry and Chilton [20]):

$$\lambda_i = \mu_i 4.1890 \times 10^{-4} \left(\mathrm{Cp}_i 2.394 \times 10^{-4} + \frac{2.48}{M_i} \right)$$

The following expression was used for computing the mixture thermal conductivity (Perry and Chilton [20]),

$$\lambda_\mathrm{f} = \frac{\sum_i y_i \lambda_i M_i^{1/3}}{\sum_i y_i M_i^{1/3}}$$

A.3. Heat capacity

The fluid mass heat capacity is calculated as

$$\mathrm{Cp}_\mathrm{f} = \frac{\sum_i M_i y_i \mathrm{Cp}_i}{\sum_i M_i y_i},$$

where the pure component heat capacities (Cp_i) were obtained from Reid et al. [19].

Appendix B. Insulation model

In the thermally insulated reactor case, a heat loss towards the outside is considered modeling the energy transfer by conduction through the insulation material, and by convection and radiation from the insulation surface to the environment.

In Eq. (2), Q^rx represents the heat flow per unitary reactor bed volume, and is related with the fluid temperature and the tube wall temperature by the heat transfer coefficient (h_w) determined by the Leva correlation (see Froment and Bischoff [22])

$$Q^\mathrm{rx} = \frac{4}{D_\mathrm{t}} h_\mathrm{w} (T_\mathrm{f} - T_\mathrm{w}) \tag{B.1}$$

By applying the Fourier law to a cylindrical geometry and considering that the thermal conductivity varies with temperature, the heat flow by conduction through the insulation material results in the following expression

$$Q^{\mathrm{rx}} = \frac{8}{D_{\mathrm{t}}^2 \ln(D_{\mathrm{ins}}/D_{\mathrm{t}})} \int_{T_{\mathrm{ins}}}^{T_{\mathrm{w}}} k(T)\mathrm{d}T \tag{B.2}$$

Finally, the heat flow is related to the heat loss from insulation surface by convection (B.4) and radiation (Eq. (B.5)) (see Koenig [26]).

$$Q^{\mathrm{rx}} = \frac{4D_{\mathrm{ins}}}{D_{\mathrm{t}}^2}(q_{\mathrm{cv}} + q_{\mathrm{rad}}) \tag{B.3}$$

$$q_{\mathrm{cv}} = 2.3613 \times 10^{-4} \left(\frac{1}{D_{\mathrm{ins}}}\right)^{0.2} \times \left(\frac{1}{(T_{\mathrm{amb}} + T_{\mathrm{ins}})0.9 - 459.67}\right)^{0.181} (T_{\mathrm{ins}} - T_{\mathrm{amb}})^{1.266} \tag{B.4}$$

$$q_{\mathrm{rad}} = \sigma\varepsilon_{\mathrm{ins}}((T_{\mathrm{ins}} + 273.16)^4 - (T_{\mathrm{amb}} + 273.16)^4) \tag{B.5}$$

References

[1] L.F. Brown, Int. J. Hydrogen Energy 26 (2001) 381–397.
[2] M. Krumpelt, T.R. Krause, J.D. Carter, J.P. Kopasz, S. Ahmed, Catal. Today 77 (2002) 3–16.
[3] A. Haryanto, S. Fernando, N. Murali, S. Adhikari, Energy Fuels 19 (2005) 2098–2106.
[4] J.R. Mielenz, Curr. Opin. Microbiol. 4 (2001) 324–329.
[5] J.M. Zalc, D.G. Löffler, J. Power Sources 111 (2002) 58–64.
[6] J.S. Campbell, Ind. Eng. Chem. Process. Des. Develop. 9 (1970) 588–595.
[7] R.L. Keiski, T. Salmi, V.J. Pohjola, Chem. Eng. J. 48 (1992) 17–29.
[8] W. Ruettinger, O. Ilinich, R.J. Farrauto, J. Power Sources 118 (2003) 61–65.
[9] D.G. Löffler, S.D. McDermott, C.N. Renn, J. Power Sources 114 (2003) 15–20.
[10] C.P.P. Singh, D.N. Saraf, Ind. Eng. Chem. Process. Des. Dev. 16 (1977) 313–319.
[11] Y. Choi, H.G. Stenger, J. Power Sources 124 (2003) 432–439.
[12] J.L. Ayastuy, M.A. Gutiérrez-Ortiz, J.A. González-Marcos, A. Aranzabal, J.R. González-Velasco, Ind. Eng. Chem. Res. 44 (2005) 41–50.
[13] M. Levent, Int. J. Hydrogen Energy 26 (2001) 551–558.
[14] G. Kim, J.R. Mayor, J. Ni, Chem. Eng. J. 110 (2005) 1–10.
[15] A.S. Quiney, G. Germani, Y. Schuurman, J. Power Sources 160 (2006) 1163–1169.
[16] A. Brunetti, Barbieri, E. Drioli, K.-H. Lee, B. Sea, D.-W. Lee, Chem. Eng. Process. 46 (2007) 119–126.
[17] P. Giunta, N. Amadeo, M. Laborde, J. Power Sources 156 (2006) 489–496.
[18] S. Hwang, R. Smith, Chem. Eng. Sci. 59 (2004) 4229–4243.
[19] R.C. Reid, J.M. Prausnitz, B.E. Poling, The Properties of Gases and Liquids, fourth ed., McGraw-Hill, New York, 1987.
[20] R.H. Perry, C.H. Chilton, Chemical Engineering Handbook, fifth ed., McGraw-Hill, New York, 1973.
[21] C.N. Satterfield, Mass Transfer in Heterogeneous Catalysis, MIT Press, Cambridge, 1970.
[22] G.F. Froment, K.B. Bischoff, Chemical Reactor Analysis and Design, second ed., Wiley, New York, 1990.
[23] gPROMS, Introductory User Guide (Release 2.3). Process Systems Enterprise Ltd., 2004.
[24] J.A. Francesconi, M.C. Mussati, E.E. Miro, R.O. Mato, P.A. Aguirre, in: Proceedings of ENPROMER 2005, Rio de Janeiro (Brazil). Paper Code: 735.
[25] S. Kovenklioglu, G.B. DeLancey, Chem. Eng. Sci. 34 (1979) 150–153.
[26] A.R. Koenig, Chem. Eng. 8 (1980) 125–128.